Liquid part of the phase diagram and percolation line for two-dimensional Mercedes-Benz water

T. Urbic

Phys. Rev. E **96**, 032122 — Published 15 September 2017

DOI: 10.1103/PhysRevE.96.032122

The liquid part of phase diagram and percolation line for the two-dimensional Mercedes–Benz water

T. Urbic

Faculty of Chemistry and Chemical Technology,

University of Ljubljana, Vecna Pot 113,1000 Ljubljana, Slovenia

Abstract

Monte Carlo simulations and Wertheim's thermodynamic perturbation theory (TPT) were used to predict the phase diagram and percolation curve for the simple two-dimensional Mercedes–Benz (MB) model of water. The MB model of water is quite popular for explaining water properties, but the phase diagram was not reported till now. In the MB model, water molecules are modeled as two-dimensional (2D) Lennard-Jones disks, with three orientation-dependent hydrogen-bonding arms, arranged as in the MB logo. The liquid part of phase space was explored using grand canonical Monte Carlo simulations and two different versions of Wertheim's thermodynamic perturbation theory for associative fluids which were used before to predict the properties of the simple MB model. We found that the theory reproduced well the physical properties of hot water, but was less successful at capturing the more structured hydrogen bonding that occurs in cold water. In addition to reporting the phase diagram and percolation curve of the model, it is also shown that improved TPT predicts the phase diagram rather well while the standard one predicts a phase transition at lower temperatures. For the percolation line, both versions have problems predicting the correct position of the line at high temperatures.

I. INTRODUCTION

Water is the most important fluid in nature for life, [1, 2] as well as for technological processesm being one of the most important liquids in industry. Water exhibits many anomalous properties that affect life at a larger scale. Mammals benefit from the large latent heat of water to cool them down through sweating. Waters large heat capacity prevents local temperature fluctuations, facilitating thermal regulation of organisms. Water has almost universal solvent action[3]. Nearly all known chemical substances will dissolve in water at least to a small extent. Water is one of the most corrosive substances known and yet is physiologically harmless. In comparison to other liquids, it has the most puzzling behavior [3, 4]. The most known examples are its density maximum at 4 °C, lower density of the solid phase compared to the liquid phase, high and nearly constant heat capacity in the liquid phase negative expansion coefficient below the temperature of the density maximum, as well as high surface tension and viscosity. The compressibility and specific heat increase anomalously by cooling. Water also has unusually high boiling, freezing and critical points. These properties are largely governed by the formation of hydrogen bonds (HB). An understanding of the hydrogen bonding is therefore crucial to understand the behavior and properties of water and aqueous solutions. A key goal of liquid–state statistical thermodynamics is to develop a quantitative theories for water and aqueous solutions (for reviews see[3–12]). A large number of models of varying complexity have been developed and analyzed to model waters extraordinary properties (for reviews, see, e.g. [13–16]), but none of the current models can correctly reproduce all physical properties of water. In principle, the properties of water can be determined with quantum-mechanical calculations[17, 18]. While they offer the highest degree of exactness, a high computational cost of these approaches limits their use to small water systems, but these insights should allow for the development and fine-tuning of simplified water models.[19–21] There have been two main approaches to modeling liquids. One approach is to perform computer simulations of atomically detailed models. These models aim for realistic detail and include variables describing van der Waals and Coulomb interactions, hydrogen bonding, etc. (reviewed in [10]). Such approaches can depend critically on the force–field used in the calculation[22, 23]. However, many properties of water and aqueous solutions can also be captured by simpler models[24, 25]. One class of such simpler models has been developed by Nezbeda and coworkers[14, 26,

27]. One the simplest models for water is the so-called Mercedes–Benz (MB) model,[28–32] which was originally proposed by Ben–Naim in 1971 [33, 34]. This is a 2-dimensional model. Each water molecule is modeled as a disk that interacts with other such waters through: (1) a Lennard–Jones (LJ) interaction and (2) an orientation–dependent hydrogen bonding interaction through three radial arms arranged as in the Mercedes–Benz (MB) logo. Interest in simplified models is due to insights that are not obtainable from all-atom computer simulations. Simpler models are more flexible in providing insights and illuminating concepts, and they do not require big computer resources. Second, simple models can explore a much broader range of conditions and external variables. Whereas simulating a detailed model may predict the behavior at a single temperature and pressure, a simpler model can be used to study a whole phase diagram of temperatures and pressures. Third, analytical models can provide functional relationships for engineering applications and lead to improved models of greater computational efficiency. Fourth, simple models can be used as a polygon to develop and study theoretical methods. Our interest in using the MB model is that it serves as one of the simplest models of an orientationally-dependent liquid, so it can serve as a testbed for developing analytical theories that might ultimately be useful for more realistic models. Another advantage of the MB model, compared to more realistic water models, is that the underlying physical principles can be more readily explored and visualized in two dimensions. For the MB model, NPT Monte Carlo simulations have shown that the MB model predicts qualitatively the density anomaly, the minimum in the isothermal compressibility as a function of temperature, the large heat capacity, as well as the experimental trends for the thermodynamic properties of solvation of nonpolar solutes[29, 31, 32, 35] and cold denaturation of proteins[36]. The 2D MB model was also extended to 3D by Bizjak et al.[37, 38] and Dias et al.[35, 39] and studied using computer simulations [35, 37–39]. The 2D model was also extensively studied with analytical methods like integral equation and thermodynamic perturbation theory[40–45]. In spite of all the Monte Carlo calculations, the phase diagram and percolation curve of the model was never calculated and this is the aim of this work, determination of the percolation line and liquid-gas coexistence line.

Even though computer simulations play an important role in understanding the properties of liquids, they can be quite time consuming, even for simple two-dimensional 2D models. So it is equally important to develop simplified, more analytical approaches. For MB water,

theories that have been developed for fluids comprised of molecules that associate into dimers and higher clusters can be applied. Wertheim[52–55] proposed his statistical–mechanical approach for strongly associating systems of molecules and a corresponding thermodynamic perturbation theory. In previous work [40–47], we applied Wertheim's theory for associating fluids[52, 53] to the MB model and some other simple models through both a thermodynamic perturbation theory (TPT) and orientationally averaged and angle-dependent integral equation theories (IET). We found that both TPT and IET approaches gave good quantitative agreement with NPT Monte Carlo results for the molar volume, isothermal compressibility, and other thermodynamic properties as a function of temperature. It is also possible to use even more analytical theories for MB-like models which are allowing the inclusion of orientation-dependent hydrogen bonding within a framework that is simple and nearly analytical. On such model is a statistical mechanical model, developed by Urbic and Dill's (UD) [48]. The model is directly descendant from a treatment of Truskett and Dill (TD), who developed a nearly analytical version of the 2D MB model [49, 50]. In the model each water molecule interacts with its neighboring waters through a van der Waals interaction and an orientation-dependent interaction that models hydrogen bonds. In this work, we applied standard [40] and improved [44] TPT for calculating the phase diagram and percolation curve. Correctness of both methods was assessed by comparison with Monte Carlo simulation results.

II. THE MODEL

In the MB model of water, water molecules are represented as a 2D disk with three arms separated by a fixed angle of 120°[29, 33], mimicking formation of hydrogen bonds. The water-water interaction potential between particles i and j is the sum of a Lennard–Jones term and a hydrogen–bonding (HB) term

$$U(\overrightarrow{X_i}, \overrightarrow{X_j}) = U_{LJ}(r_{ij}) + U_{HB}(\overrightarrow{X_i}, \overrightarrow{X_j}) \tag{1}$$

where r_{ij} is the distance between centers of particles i and j, $\overrightarrow{X_i}$ is the vector representing the coordinates and orientation of the i^{th} particle. The Lennard–Jones part of the potential is determined using the standard form

$$U_{LJ}(r_{ij}) = 4\varepsilon_{LJ}\left((\frac{\sigma_{LJ}}{r_{ij}})^{12} - (\frac{\sigma_{LJ}}{r_{ij}})^{6}\right), \tag{2}$$

where ε_{LJ} is the depth of the LJ part of potential and σ_{LJ} is the contact value. The hydrogen bonding part of the potential is the sum of interactions U_{HB}^{kl} between arms of different molecules

$$U_{HB}(\vec{X}_i, \vec{X}_j) = \sum_{k,l=1}^{3} U_{HB}^{kl}(r_{ij}, \theta_1, \theta_2). \tag{3}$$

This interaction is a Gaussian function in distance and both angles

$$\begin{aligned} U_{HB}^{kl}(r_{ij}, \theta_1, \theta_2) &= \varepsilon_{HB} G(r_{ij} - r_{HB}) G(\vec{i_k}\vec{u_{ij}} - 1) G(\vec{j_l}\vec{u_{ij}} + 1) & (4) \\ &= \varepsilon_{HB} G(r_{ij} - r_{HB}) G(\cos(\theta_i + \tfrac{2\pi}{3}(k-1)) - 1) G(\cos(\theta_j + \tfrac{2\pi}{3}(l-1)) + 1) & (5) \end{aligned}$$

$\varepsilon_{HB} = -1$ is a HB energy parameter and $r_{HB} = 1$ is a characteristic HB length. $\overrightarrow{u_{ij}}$ is the unit vector along $\overrightarrow{r_{ij}}$ and $\overrightarrow{i_k}$ is the unit vector representing the k^{th} arm of the i^{th} particle, where θ_i is the orientation of the i^{th} particle and $G(x)$ is an unnormalized Gaussian function

$$G(x) = \exp\left(-\frac{x^2}{2\sigma^2}\right). \tag{6}$$

The strongest hydrogen bond occurs when an arm of one particle is co–linear with the arm of another particle and the two arms point in opposing directions. The LJ well–depth ε_{LJ} is 0.1 times the HB interaction energy ε_{HB} and the Lennard–Jones contact parameter σ_{LJ} is $0.7 r_{HB}$. The width of the Gaussian for distances and angles ($\sigma = 0.085 r_{HB}$) is small enough that a direct hydrogen bond is more favorable than a bifurcated one.

III. MONTE CARLO COMPUTER SIMULATION

To calculate the phase diagram and study percolation properties, we performed Monte Carlo simulations in the grand canonical ensemble (constant μ, V , and T)[56]. The periodic boundary conditions and the minimum image convention were used to mimic an infinite system of particles. Starting configurations were selected randomly. In each move, we randomly tried to translate or rotate random particle, or insert or remove random particle. Probabilities for translation, rotation and exchange of particles were the same. In one cycle, we tried to translate and rotate each particle on average, and to make as many insertions and removals as the average number of particles in the system. The simulations were allowed to equilibrate for 50000 cycles and averages were taken for 20 series, each consisted for another 50000 cycles to obtain well-converged results. In the system we had from 50 to 500 particles depending on the density of the system. Note that 100 molecules in 2D is equivalent to 1000

particles in 3D. Thermodynamic quantities such as energy were calculated as statistical averages over the course of the simulations [56]. The cut off of the potential was the half-length of the simulation box. Increasing the number of particles had no significant effect on the calculated quantities. In addition to the MB water simulations described above, we also performed simulations in the canonical (NVT) ensemble [56]. One purpose of this calculation was to calculate pressure by means of the virial equation [56] and to perform the cluster analysis which is used to classified the overall bonding state of the system. The cluster and bond analyses use an energy criteria wherein water molecules are considered bonded when their hydrogen bonded energy is less than -0.05. Small variations of this energy cutoff did not account for significant differences in the bonding state of the system. The percolation line was determined as the density at which at least 50% of water particles were part of one big cluster connected by hydrogen bonds.

IV. THERMODYNAMIC PERTURBATION THEORY

Here is a brief overview of Wertheim's first order perturbation theory[52, 57], used previously[40, 41, 44]. The Helmholtz free energy for MB molecules is a sum of an ideal term, A_{id}, a reference term, A_{LJ}, and a perturbation term, A_{HB}. The latter takes into account the association of MB molecules into hydrogen bonded networks

$$\frac{A}{Nk_BT} = \frac{A_{id}}{Nk_BT} + \frac{A_{LJ}}{Nk_BT} + \frac{A_{HB}}{Nk_BT} \tag{7}$$

where N is the number of particles, T is temperature, and k_B is Boltzmann's constant. The term A_{LJ} was determined using the Barker–Henderson (BH) perturbation theory [40, 51]. The use of other perturbation methods for the Lennard–Jones part did not improve the results. In BH theory, the reference system was the hard disks system

$$\frac{A_{LJ}}{Nk_BT} = \frac{A_{HD}}{Nk_BT} + \frac{\rho}{2k_BT}\int_{\sigma_{LJ}}^{\infty} g_{HD}(r,\eta)u_{LJ}(r)d\overrightarrow{r} \tag{8}$$

where A_{HD} is the hard–disk part of the Helmholtz free energy, ρ is the number density of water particles, η is the packing fraction of the hard disk reference system, and $g_{HD}(r,\eta)$ is the pair distribution function of the hard disk reference fluid [40]. We calculated the contribution of hydrogen bonding to the Helmholtz free energy using

$$\frac{A_{HB}}{Nk_BT} = 3(\log x - \frac{x}{2} + \frac{1}{2}) \tag{9}$$

where x is the fraction of molecules not bonded at one particular arm. x is obtained from the mass–action law [52] in the form

$$x = \frac{1}{1 + 3\rho x \Delta}. \tag{10}$$

Finally, Δ is defined by [52, 57]

$$\Delta = 2\pi \int g_{LJ}(r, \rho) \bar{f}_{HB}(r) r dr \tag{11}$$

where $\bar{f}_{HB}(r)$ is an orientationally averaged Mayer function for the hydrogen–bonding potential of one site. The pair distribution function $g_{LJ}(r)$ is obtained by solving the Percus–Yevick equation for Lennard–Jones disks. Once the Helmholtz free energy is known, other thermodynamic quantities may be calculated using standard thermodynamic relations [51].

In the improved TPT,[44] the difference to standard TPT is that, instead of the density ρ, we use the effective density ρ^{ef} in Eq. (7)–(11) as an effective density, which is calculated as explained below. The logic for this is than the particles cannot access the whole space in the system when they form bonds. When two water molecules form a hydrogen bond, it sterically occludes space, which becomes inaccessible to any other molecule (see Figure 2). The effective particle volume was calculated as

$$V^{ef} = \frac{1}{\rho} - \frac{\bar{n} V'}{2} \tag{12}$$

where V' is the volume not accessible to other molecules when two molecules form a hydrogen bond and can be approximated by simple geometry. Two water molecules that form a hydrogen bond are separated by a distance 1. If the LJ core is approximated by diameter d of HD molecules from BH perturbation theory, V' can be approximated as

$$V' = \sqrt{d^2 - \frac{1}{2}} - \frac{\pi d^2}{4} \tag{13}$$

In equation (12), $\bar{n}$ is the average number of hydrogen bonds per molecule. Each molecule has 3 arms. The probability that a hydrogen bond is formed at one arm is $(1 - x)$, where x is the ratio of non-bonded molecules at one arm. We now get:

$$\bar{n} = 3(1 - x). \tag{14}$$

The effective particle density can now be calculated as

$$\rho^{ef} = \frac{1}{V^{ef}}. \tag{15}$$

Now, the set of equations (10)-(15) must be solved iteratively to get the effective density, ρ^{ef}, and the fraction of molecules x that are not hydrogen bonded. The effective packing fraction is then calculated as $\eta^{ef} = \rho^{ef}\pi d^2/4$. Once the effective density and packing fraction are known, the Helmholtz free energy can be calculated with equations (7)-(9) and other thermodynamic properties with standard thermodynamic relations [51].

V. RESULTS AND DISCUSSION

All our results reported below are shown in reduced units; the excess internal energy and temperature are normalized to the HB energy parameter ε_{HB} ($A^* = \frac{A}{|\varepsilon_{HB}|}, T^* = \frac{k_B * T}{|\varepsilon_{HB}|}$) and the distances are scaled to the hydrogen bond characteristic length r_{HB} ($r^* = \frac{r}{r_{HB}}$). Errors in the MC simulations are the size of the symbols used to present data points.

In first step, we determined the gas-liquid part of the phase diagram for the MB model of water by computer simulation. We did this by performing Monte Carlo simulations in the grand canonical ensemble. We calculated dependence of density as a function of chemical potential at constant temperature. Results for selected temperatures are plotted in Figure 3a as points. For temperatures above the critical point the function is smooth, while for temperatures below we observe a jump in density between the gas and liquid density, which are in coexistence. In Figure 3a we also plotted results from the improved TPT. For the high temperature $T^* = 0.3$ (green line and symbols) TPT reproduces the MC data very well for densities up to 1. At the mid range temperature $T^* = 0.2$ (blue line and symbols) we can observe similar agreement, while at cold temperature $T^* = 0.15$ (pink line and symbols) the improved TPT shows phase transition behavior. At all temperatures there is disagreement between TPT and MC results at high densities, where improved the TPT starts to fail. In improved and standard TPT, we can determine gas and liquid phases which coexist by doing a Maxwell construction for the chemical potential as a function of volume (inverse density). Another way to determine this is by plotting the pressure as a function of density, which is plotted in Figure 3b for different temperatures. In Monte Carlo simulations, the pressure was calculated using a virial route in the NVT ensemble. Agreement between the improved TPT and MC data is similar to those observed for the chemical potential. Also, here we can do Maxwell construction for determining liquid-gas coexistence densities. To further test the improved TPT, we checked how good TPT is in reproducing the internal energy U^*. The

comparison is plotted in Figure 3c. We can see that agreement is quantitative, TPT can predict correct trends, but cannot predict correct values exactly. An alternative to doing Maxwell construction to determine the gas-liquid coexistence densities for both versions of TPT is by plotting the chemical potential as a function of pressure. The curve in the region below the critical point intersects at the coexistence pressure, as demonstrated in Figure 3d (temperature below critical temperature has intersection while curve above does not). Doing these calculations for both versions of TPT and MC simulations, we were able to determine the gas-liquid coexistence lines, which are plotted in Figure 4. This figure shows a comparison of the gas-liquid equilibria curves calculated by MC and both TPT methods. The critical point for the gas-liquid transition by MC is T_c^*=0.18, p_c^*=0.016 $\mu_c^* = -0.56$ and ρ_c^*=0.433, by standard TPT is T_c^*=0.14, p_c^*=0.0036, $\mu_c^* = -0.625$ and ρ_c^*=0.150 and by improved TPT is T_c^*=0.179, p_c^*=0.017, $\mu_c^* = -0.533$ and ρ_c^*=0.370. We can see that the improved TPT predict the correct critical point rather well, while the standard TPT predicts it at a lower temperature, density and pressure. The reasons include the position of the arms, which are not on the surface of LJ disk, but further away from the surface. Due to this there is a part of space inaccessible for molecules which is corrected in the improved TPT. We also checked the possibility for a liquid-liquid phase transition of the model, but due to crystallization issues we cannot calculate this with the current version of the MC method, both TPT methods fail to detect any liquid-liquid phase transition.

We continued our study toward determining the percolation line, first by calculating the ratios of molecules with 0, 1, 2 and 3 hydrogen bonds. In the MC simulation, we analyze the average number of water molecules forming 0, 1 2 and 3 hydrogen bonds during the MC run. In TPT, we calculate this from the fraction of molecules not bonded at one particular arm x as $x_0 = x^3$, $x_1 = 3x^2(1-x)$, $x_2 = 3x(1-x)^2$ and $x_3 = (1-x)^3$. Results for different temperatures are presented in Figure 5. TPT results are presented for the standard version of TPT. Predictions for the fraction are semi-accurate. Surprisingly, the agreement for the ratio of molecules with no hydrogen bonds is worst for higher temperatures. TPT is doing quite well for one and two bonded molecules for all temperatures and densities. The worst agreement is for molecules with three hydrogen bonds, where we have bad agreement for all temperatures and densities. Next we checked how the system is connected by hydrogen bonds. We performed cluster analysis and checked the fraction of water molecules belonging to the biggest cluster in the system by MC computer simulations. Results for this are plotted

in Figure 6. At constant temperature, the fraction of molecules belonging to the biggest cluster connected by hydrogen bonds increases with density, reach a maximum and then, due to high packing, starts to decrease. This happens at densities higher than the perfect hexagonal crystal. In MC, the percolation line was determined as density at which at least 50% of water particles were part of one big cluster connected by hydrogen bonds. In TPT, we followed Bianchi et al. [58] where the ratio of non-bonded particles at a particular arm at percolation x_p is equal to 0.5. Percolation curves determined with these methods are presented in Figure 7 for MC simulations and both versions of TPT. We can see that since the calculation in TPT is based on ratios of free particles, and since agreement with MC was not good for high temperatures, the TPT curves deviate from MC results in that region. The TPT is predicting a connected system at lower temperatures than MC.

VI. CONCLUSIONS

Monte Carlo simulations and Wertheim's thermodynamic perturbation theory were used to predict the phase diagram and percolation curve of the simple Mercedes–Benz (MB) model of water. The MB model balances Lennard-Jones interactions with an orientation-dependence that is intended to mimic hydrogen-bonding. The MB model has previously been shown to have the volume anomalies of pure water and the thermal anomalies of nonpolar solvation. The TPT method is orders of magnitude more efficient than the Monte Carlo simulations. We have determined the liquid-gas part of the phase diagram and percolation curve and pinpointed the area where we have gas-liquid coexistence and the phase space where the system is connected by hydrogen bonds. For the MB model of water, we did not observe any liquid-liquid phase transition in the area of observation by MC and TPT. If it exists, it is present in the sopercooled region, but in MC this is difficult to study due to crystalization. We found that the improved TPT method reproduced well the physical properties of water in the area of the phase transition investigated while standard TPT is predicting a coexistence at lower temperatures. Both theories are able to predict the percolation line at lower temperatures, while failing to predict it at high temperatures. The TPT methods have error in the prediction of ratio of non-bonded particles at one arm. This error magnifies at higher temperatures when calculating percolation curve.

Acknowledgments

This work was supported by the NIH (GM063592) and Slovenian Research Agency (P1 0103-0201, N1-0042) and the National Research, Development and Innovation Office of Hungary (SNN 116198).

---

[1] M. Chaplin, Nat. Rev. Mol. Cell Biol. **7**, 861 (2006).

[2] M. J. Tait, F. Franks, Nature **230**, 91 (1971).

[3] F. Franks., Ed. *Water, a Comprehensive Treatise*, (Plenum Press, New York, 1972–1980) Vol. 1–7.

[4] D. Eisenberg and W. Kauzmann, *The structure and properties of water* (Oxford University Press, Oxford, 1969).

[5] F. H. Stillinger, Science **209**, 451 (1980).

[6] C. Tanford, *The hydrophobic effect: formation of micelles and biological membranes*, 2nd ed. (Wiley, New York, 1980).

[7] W. Blokzijl and J. B. F. N. Engberts, Angew. Chem. Int. Ed. Engl. **32**, 1545 (1993).

[8] G. Robinson, S.–B. Zhu, S.Singh and M. Evans, *Water in Biology, Chemistry and Physics: Experimental Overviews and Computational Methodologies* (World Scientific, Singapore, 1996).

[9] R. Schmidt, Monatshefte für Chemie **132**, 1295 (1993).

[10] B. Guillot, J. Mol. Liquids **101**, 219 (2002).

[11] A. Ben-Naim, Biophys. Chem. **105**, 183 (2003).

[12] L. R. Pratt, Annu. Rev. Phys. Chem. **53**, 409 (2002).

[13] W. L. Jorgensen, J. Chandrasekhar, J. D. Madura, R. W. Impey, and M. L. Klein, J. Chem. Phys. **79**, 926 (1983).

[14] I. Nezbeda, J. Mol. Liq. **73/74**, 317 (1997).

[15] B. Guillot, J. Mol. Liq. **101**, 219 (2002).

[16] C. Vega, J. L. F. Abascal, M. M. Conde, and J. L. Aragones, Faraday Discuss. **141**, 251 (2009).

[17] K. B. Lipkowitz, D. B. Boyd, S. J. Smith, and B. T. Sutcliffe, Rev. Comput. Chem. **10**, 271 (2007).

[18] E. J. Baerends and O. V. Gritsenko, J. Phys. Chem. A **101**, 5383 (1997).

[19] D. van der Spoel, P. J. van Maaren, and H. J.C. Berendsen, J. Chem. Phys. **108**, 10220 (1998).

[20] H. W. Horn, W. C. Swope, J. W. Pitera, J. D. Madura, T. J. Dick, G. L. Hura, and T. Head-Gordon, J. Chem. Phys. **120**, 9665 (2004).

[21] J. L.F. Abascal and C. Vega, J. Chem. Phys. **123**, 234505 (2005).

[22] J-C. Soetens, C. Millot, C. Chipot, G. Jansen, J. G. Angyán and B. Maigret, J. Phys. Chem. B **101**, 10910 (1997).

[23] B. Hess and Nico F. A. van der Vegt, J. Phys. Chem. B **110**, 17616 (2006).

[24] T.M. Truskett, P.G. Debenedetti, S. Sastry, and S. Torquato, J. Chem. Phys. **111**, 2647 (1999).

[25] K.A. Dill, T.M. Truskett, V. Vlachy, and B. Hribar-Lee, Ann. Rev. Biophys. Biomolec. Struc. **34**, 173 (2005).

[26] I. Nezbeda, J. Kolafa and Yu. V. Kalyuzhnyi, Mol. Phys. **68**, 143 (1989).

[27] I. Nezbeda and G. A. Iglezias–Silva, Mol. Phys. **69**, 767 (1990).

[28] G. Andaloro and R. M. Sperandeo–Mineo, Eur. J. Phys. **11**, 275 (1990).

[29] K. A. T. Silverstein, A. D. J. Haymet and K. A. Dill, J. Am. Chem. Soc. **120**, 3166 (1998).

[30] K. A. T. Silverstein, K. A. Dill, and A. D. J. Haymet, Fluid Phase Equilibria **120**, 3166 (1998).

[31] N. T. Southall and K. A. Dill, J. Phys. Chem. B **104**, 1326 (2000).

[32] K. A. T. Silverstein, A. D. J. Haymet and K. A. Dill, J. Chem. Phys. **114**, 6303 (2001).

[33] A. Ben–Naim, J. Chem. Phys. **54**, 3682 (1971).

[34] A. Ben–Naim, Mol. Phys. **24**, 705 (1972).

[35] C. L. Dias, T. Hynninen, T. Ala–Nissila, A. S. Foster and M. Karttunen, J. Chem. Phys. **134**, 065106 (2011).

[36] C. L. Dias, Phys. Rev. Lett. **109**, 048104 (2012).

[37] A. Bizjak, T. Urbic, V. Vlachy, and K. A. Dill, Acta Chim. Slov. **54**, 532 (2007).

[38] A. Bizjak, T. Urbic, V. Vlachy and K. A.Dill, J. Chem. Phys. **131**, 194504 (2009).

[39] C. L. Dias, T. Ala-Nissila, M. Grant and M. Karttunen, J. Chem. Phys. **131**, 054505 (2009).

[40] T. Urbic, V. Vlachy, Yu. V. Kalyuzhnyi, N. T. Southall and K. A. Dill, J. Chem. Phys. **112**, 2843 (2000).

[41] T. Urbic, V. Vlachy, Yu. V. Kalyuzhnyi, N. T. Southall and K. A. Dill, J. Chem. Phys. **116**, 723 (2002).

[42] T. Urbic, V. Vlachy, Yu. V. Kalyuzhnyi and K. A. Dill, J. Chem. Phys. **118**, 5516 (2003).

[43] T. Urbic, V. Vlachy, O. Pizio, K. A. Dill, J. Mol. Liq. **112**, 71 (2004).

[44] T. Urbic, V. Vlachy, Yu. V. Kalyuzhnyi and K. A. Dill, J. Chem. Phys. **127**, 174511 (2007).

[45] T. Urbic and M. F. Holovko, J. Chem. Phys. **135**, 134706 (2011).

[46] T. Urbic, J. Mol. Liq. **228**, 32 (2017).

[47] T. Urbic, J. Mol. Liq. **238**, 129 (2017).

[48] T. Urbic and K. A. Dill, J. Chem. Phys. **132**, 224507 (2010).

[49] T. M. Truskett and K. A. Dill, J. Chem. Phys. **117**, 5101 (2002).

[50] T. M. Truskett and K. A. Dill, J. Phys. Chem. B **106**, 11829 (2002).

[51] J. P. Hansen and I. R. McDonald,*Theory of Simple Liquids* (Academic, London, 1986).

[52] M.S. Wertheim, J. Stat. Phys. **42**, 459, 477 (1986).

[53] M. S. Wertheim, J. Chem. Phys. **87**, 7323 (1987).

[54] M. S. Wertheim, J. Chem. Phys. **88**, 1145 (1987).

[55] M. S. Wertheim, J. Chem. Phys. **85**, 2929 (1986).

[56] D. Frenkel and B. Smit, *Molecular simulation: From Algorithms to Applications*, (Academic Press, New York, 2000).

[57] G. Jackson, W. G. Chapman and K. E. Gubbins, Mol. Phys. **65**, 1 (1988).

[58] E. Bianchi, P. Tartaglia, E. Zaccarelli and F. Sciortino, J. Chem. Phys. **128**, 144504 (2008).

CAPTIONS TO THE FIGURES.

Figure 1. The MB molecules. Particles form the strongest hydrogen bond when arms are collinear and the distance between two particles is equal to r_{HB}.

Figure 2. Definition of the excluded volume in the modified version of TPT.

Figure 3. (a) Density as a function of chemical potential for different temperatures. The jump indicates a liquid-gas phase transition. (b) Pressure as a function of density for different temperatures. Below the critical point, we can see nonmonotonic behavior of pressure and, with Maxwell construction, the coexistence line can be calculated. (c) Internal energy as a function of density for different temperatures. Results in (a)-(c) from computers simulations are plotted by symbols and from the improved TPT by lines. (d) An alternative to Maxwell construction is to plot the chemical potential as a function of pressure in the region of phase transition. Results were calculated by the improved TPT method for different temperatures. The intersection of curve is where there is coexistence of phases. Green color is for high temperature $T^* = 0.3$, blue for $T^* = 0.2$ and pink for low temperature $T^* = 0.15$.

Figure 4. Vapour-liquid equilibria from MC and TPT. Results from computers simulations are plotted as symbols, from TPT as a solid line and from improved TPT as a dashed line. In (a) there is $T * -\rho^*$ liquid-gas coexistence, in (b) $T * -p^*$ coexistence and in (c) $T * -\mu^*$ coexistence.

Figure 5. Density dependence of ratios of molecules with 0, 1, 2 and 3 hydrogen bonds. Points are the results from Monte Carlo computer simulations and lines from standard TPT. Results are plotted for different temperatures (a) T^* =0.18, (b) T^* =0.22, and (c) T^* =0.3.

Figure 6. Fraction of molecules belonging to the biggest cluster as a function of density for different temperatures. Points are the results from Monte Carlo computer simulations. Red color is for high temperature $T^* = 0.4$, green for $T^* = 0.3$, blue for $T^* = 0.2$, light blue for low temperature $T^* = 0.18$, and pink for low temperature $T^* = 0.15$.

Figure 7. Percolation line from MC and TPT. Results from computers simulations are plotted as symbols and from TPT as a solid line and from improved TPT as a dashed line.

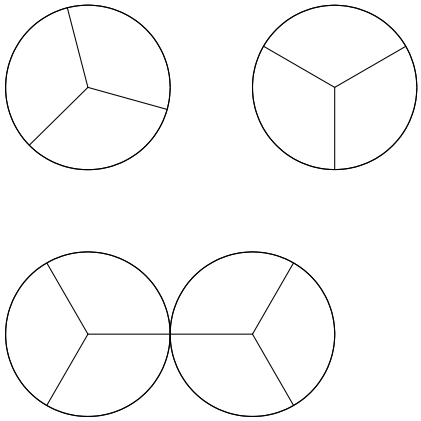

Figure 1 (Urbic et al.)

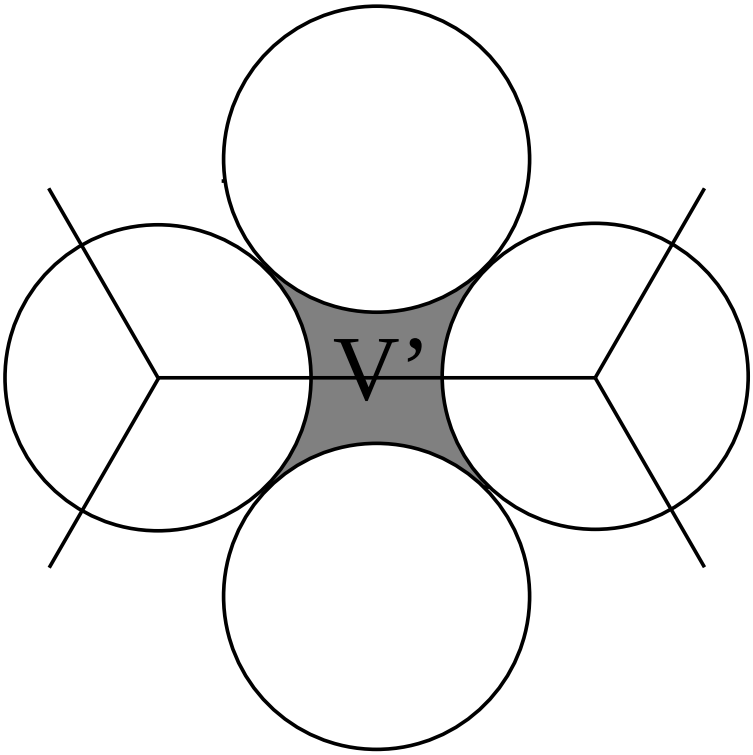

Figure 2 (Urbic et al.)

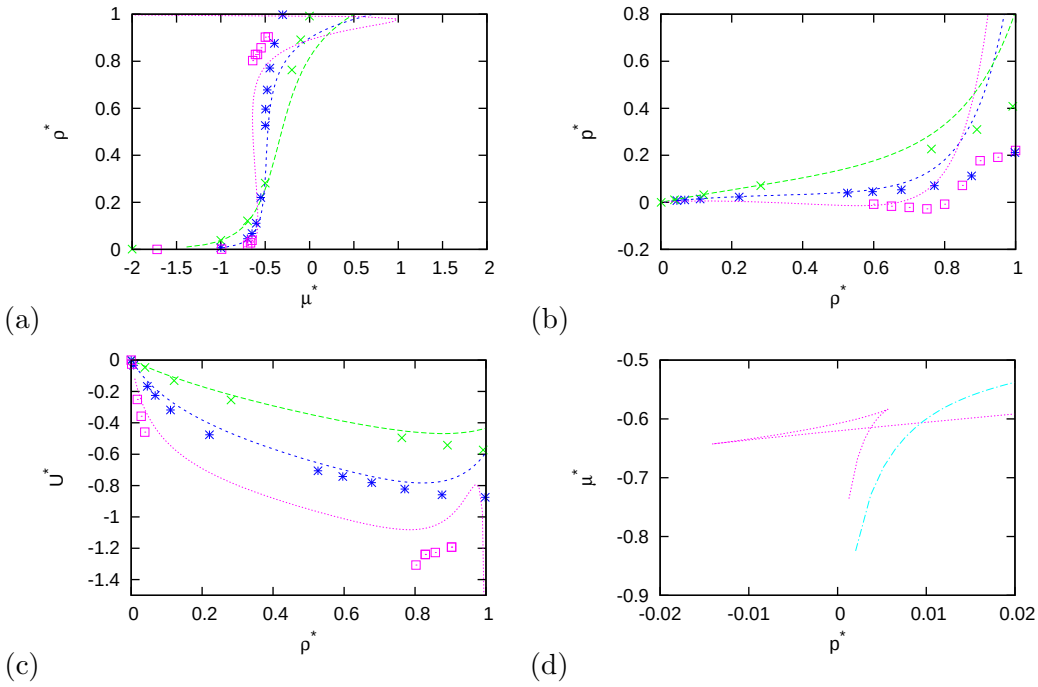

Figure 3 (Urbic et al.)

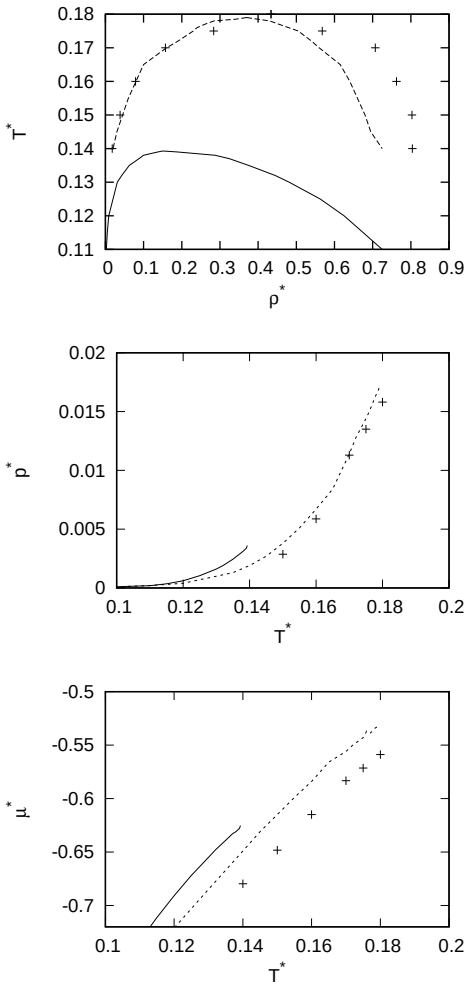

Figure 4 (Urbic et al.)

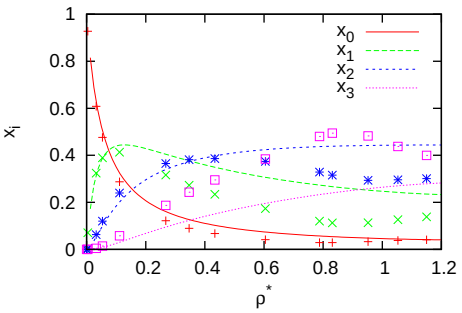

(a)

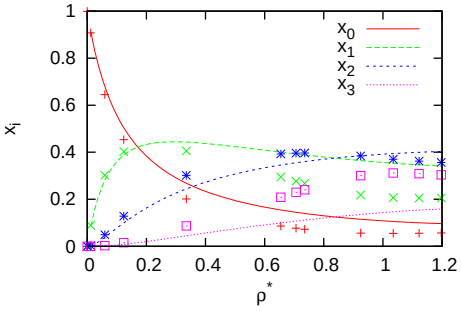

(b)

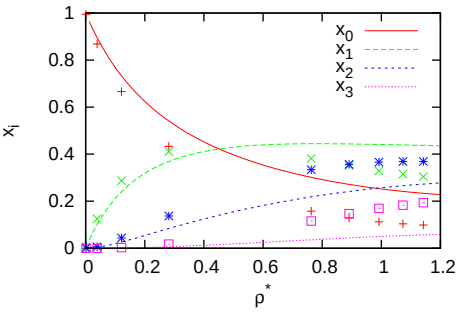

(c)

Figure 5 (Urbic et al.)

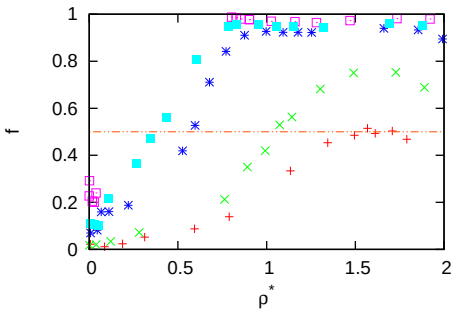

Figure 6 (Urbic et al.)

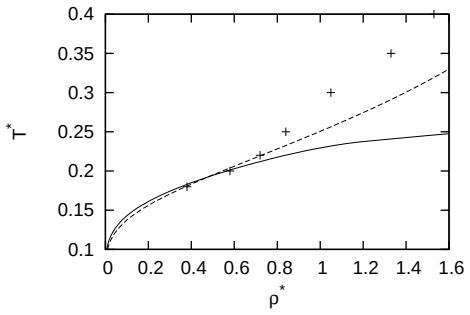

Figure 7 (Urbic et al.)